A kernel approach to deconvolution of the complex modulus in linear viscoelasticity

Davies, A. R.; Douglas, R. J.

Published in:
Inverse Problems

DOI:
10.1088/1361-6420/ab2944

Publication date:
2019

Citation for published version (APA):
Davies, A. R., & Douglas, R. J. (2019). A kernel approach to deconvolution of the complex modulus in linear viscoelasticity. *Inverse Problems*, *36*(1), [015001]. https://doi.org/10.1088/1361-6420/ab2944

A kernel approach to deconvolution of the complex modulus in linear viscoelasticity.

A.R. Davies[a,*], R.J. Douglas[b]

[a]*School of Mathematics, Cardiff University, Senghennydd Road, Cardiff CF24 4AG, UK.*
[b]*Department of Mathematics, Aberystwyth University, Aberystwyth SY23 3BZ, UK.*

Abstract

The relaxation spectrum of a viscoelastic material holds the key to describing its relaxation mechanisms at a molecular level. It also plays a fundamental role in accessing the molecular weight distribution, and in modelling the dynamics of complex fluids. The relaxation spectrum cannot be measured *directly*, but it may be locally determined from experimental measurements of viscoelastic response at a macroscopic level. In particular, the relaxation spectrum is a continuous distribution of relaxation times which may be recovered, at least locally, from measurements of the complex modulus of the material. Although mathematical expressions for the continuous spectrum have been known for well over a century, these were inaccessible to numerical implementation for decades. Regularization methods for approximating *discrete line spectra* were first introduced in the 1980s, but it was not until 2012 that methods for recovering continuous spectra in a mathematical framework were proposed. In this paper, we analyze spectrum recovery within the framework of reproducing kernel Hilbert spaces and identify such spaces as natural homes for the complex modulus and spectrum. Theorems are proved establishing the convergence of inverse operators expressed as series of derivatives of the complex modulus. This enables a detailed characterization of the native spaces of the real and imaginary parts of the complex modulus, and leads to a further theorem which identifies a hierarchy of trial spaces for the spectrum. Homeomorphic trial spaces for data and spectra are then specified in detail, and their efficacy demonstrated by means of a case study.

Keywords: linear viscoelasticity, complex modulus, native spaces, continuous relaxation spectrum, differential series, homeomorphic trial spaces.

1. Introduction

Most materials encountered in everyday life are viscoelastic in nature. Examples include polymers, plastics, composites, foods, biological fluids, oils, paints and gels. Both viscous and elastic properties pertain in these

*Corresponding author. Electronic mail: DaviesR@cardiff.ac.uk

materials, and when subjected to an applied force the resulting deformation is a combination of viscous response and elastic response. The mathematical and computational modelling of viscoelastic behaviour must enable the description of thread-like, flexible, long-chain macromolecules in motion, and an important contributor to this description is the phenomenological theory of *linear viscoelasticity.*

Linear viscoelasticity describes the relationship between stress and strain in a viscoelastic material for a restricted class of flows and deformations with very small strains and strain rates. Despite its formal limitations, the theory has a fundamental significance because certain key material functions arising in the theory also play a role in modelling more complex flows in linear and nonlinear regimes. Stress in the material depends not only on the current strain, or rate of strain, but also on past strain history. For this reason, viscoelastic materials are referred to as *materials with memory.* The relaxation processes involved can occur on a variety of different time-scales, and a key function used in the modelling is the *relaxation modulus* of the material, which is the time-decay in stress resulting from a unit step in strain. The relaxation modulus may be viewed as a superposition of separate relaxation mechanisms, each decaying on a different time-scale. The distribution of relaxation times (decay rates) associated with the relaxation modulus is called the *relaxation spectrum* of the material.

In reality, the distribution of relaxation times in a viscoelastic material is infinite. The *continuous relaxation spectrum* (CRS) and its mathematical properties will be investigated in some detail in what follows. In engineering applications, however, the spectrum is represented by a finite number (usually fewer than 10) of relaxation times. Such a spectrum is called a *discrete line spectrum* and its associated relaxation modulus is a finite sum of decaying exponential functions of time. This approximation and its associated exponential decay is a convenient tool for representing experimental data, and has led to significant advances in computational modelling. However, the approximation has its limitations (McDougall *et al* (2014); Anderssen *et al* (2015); Ankiewitz *et al* (2016)).

Relaxation spectra are important not only in describing the relaxation modulus, but also in revealing the inter-connections between the modulus and other material properties such as creep and molecular weight distribution. Neither discrete spectra nor continuous spectra can be measured *directly* by experiment, but they can be locally recovered from *indirect* measurements by solving one or more inverse problems. Previous methods of approximating the CRS have included contributions by Malkin (2006), Stadler and Bailly (2009), Stadler (2010), Davies and Goulding (2012), Cho (2013), Anderssen *et al* (2015), and Davies *et al* (2016). None of these methods take into account the precise nature of the native spaces occupied by the real and imaginary parts of the complex modulus: hence the motivation for the current paper.

In this paper, we analyze spectrum recovery within the framework of reproducing kernel Hilbert spaces, and identify such spaces as natural homes for the complex modulus and spectrum. Theorems are proved establishing the convergence of inverse operators expressed as series of derivatives of the complex modulus. This enables a detailed characterization of the native spaces of the real and imaginary parts of the complex modulus, and leads to a further theorem which identifies a hierarchy of trial spaces for the spectrum. Homeomorphic trial spaces for data and spectra are then specified in detail, and their efficacy demonstrated by means of a case study.

The paper is structured as follows. Section 2 summarizes the main mathematical concepts underpinning linear viscoelasticity, while Section 3 shows how the CRS may be recovered as series involving derivatives of the storage and loss moduli separately. Section 4 introduces new series combining derivatives of both storage and loss moduli (*mixed derivative series*), while Section 5 presents sufficient conditions and theorems for series convergence. Section 6 briefly describes how linearly mixed sequences can accelerate convergence, thereby giving improved resolution enhancement. Section 7 describes the native spaces occupied by the real and imaginary parts of the complex modulus, and Section 8 develops natural homeomorphic trial spaces for data and spectra. The case study is presented in Section 9, and conclusions drawn in Section 10.

2. Mathematical background

The mathematical theory of linear viscoelasticity originated in the latter half of the 19th century. Notable contributors were Maxwell, Meyer, Kelvin and Voigt, but by far the most significant and far-reaching contribution was made by Boltzmann. An account of the historical development of the subject, with a detailed bibliography, is to be found in the book by Tanner and Walters (1998).

In an incompressible shear deformation, Boltzmann's general linear integral model for viscoelastic materials relates the stress $\sigma(t)$ to the strain-rate $\dot{\gamma}(t)$ in the form

$$\sigma(t) = \int_{-\infty}^{t} G(t-t')\dot{\gamma}(t')dt', \tag{2.1}$$

where $G(t)$ denotes the relaxation modulus, which is a positive, monotonically decreasing, and continuously differentiable function of time. The *memory function* of the material is defined by means of the first derivative as $-\dot{G}(t)$, which, in keeping with the principle of fading memory (Saut and Joseph, 1983), is also monotonically decreasing. This means that $\dot{G}(t)$ is monotonically increasing. Bernstein's theorem (Bernstein,1928) states that successive derivatives of $G(t)$ of all orders are alternately monotonically increasing and decreasing if and only if $G(t)$ is the Laplace transform of a positive measure. Under this constraint

$G(t)$ is said to be *completely monotone* and may be written in the form

$$G(t) = G_e + \int_0^\infty H(\tau) e^{-\frac{t}{\tau}} \frac{d\tau}{\tau}, \tag{2.2}$$

where G_e is a material constant, given by

$$G_e = \lim_{t \to \infty} G(t), \tag{2.3}$$

and $H(\tau)$ is the CRS associated with a continuous range of relaxation times τ. Equation (2.2) serves as a mathematical definition of the CRS. In keeping with Bernstein's theorem it will be assumed throughout that $H(\tau) \geq 0$.

As mentioned in the introduction, relaxation spectra cannot be measured directly, but must be found from indirect measurements. A common method is to sample the *complex modulus* of the material (see equation (2.6)) at different frequencies in an oscillatory shear experiment (Walters, 1975). A small amplitude oscillatory strain is applied in the form

$$\gamma(t) = \begin{cases} \gamma_0 e^{i\omega t} & \text{if } t \geq 0; \\ 0 & \text{if } t < 0, \end{cases} \tag{2.4}$$

with constant angular frequency ω. This enables equation (2.1) to be written in the form

$$\sigma(t) = G^*(\omega)\gamma(t) + o(1), \tag{2.5}$$

where $G^*(\omega)$ defines the complex modulus (also called the *complex shear modulus*, or *dynamic modulus*) as a function of frequency. This is given by

$$G^*(\omega) = G_e + i\omega \int_0^\infty [G(t') - G_e] e^{-i\omega t'} dt'. \tag{2.6}$$

Under the transformation $z = i\omega^{-1}$ it follows from equation (2.2) that $G^*(\omega)$ is related to the CRS by the following complex Stieltjes transforms

$$G^*(\omega) = G_e + \int_0^\infty \frac{i\omega}{1 + i\omega\tau} H(\tau) d\tau = G_e + \int_0^\infty \frac{H(\tau)}{\tau - z} d\tau. \tag{2.7}$$

If $G^*(\omega)$ were measurable at all frequencies $0 < \omega < \infty$, then in principle the transform (2.7) can be inverted to yield the spectrum for all relaxation times $0 < \tau < \infty$. The oscillatory shear experiment, however, can be repeated only for a limited range of sampled frequencies, which means that exact inversion formulae based on semi-infinite intervals become problematic. Furthermore, when z is pure imaginary, as is the case in equation (2.7), then recovering the spectrum from the complex modulus is an exponentially ill-posed inverse problem, and is highly unstable to small perturbations in the data.

The real part of $G^*(\omega)$ is called the *storage modulus* and denoted by $G'(\omega)$, while the imaginary part is called the *loss modulus* and is denoted by $G''(\omega)$. These are given by the pair of Fredholm integral equations

$$G'(\omega) = G_e + \int_0^\infty \frac{\omega^2\tau^2}{1+\omega^2\tau^2} H(\tau)\frac{d\tau}{\tau} \tag{2.8}$$

$$G''(\omega) = \int_0^\infty \frac{\omega\tau}{1+\omega^2\tau^2} H(\tau)\frac{d\tau}{\tau}, \tag{2.9}$$

which are the real and imaginary parts of (2.7). The Fredholm equations (2.8) and (2.9) must share the same solution H, a property which derives from the analyticity of $G^*(\omega)$ in the right-hand complex frequency half-plane. $G'(\omega)$ and $G''(\omega)$ are related via the Kramers-Krönig relations (Tschoegl, 1989).

In modelling low frequency and high frequency response, low order moments of the relaxation spectrum play a role. The following constraints are normally imposed:

$$\lim_{\omega\to 0} \frac{G'(\omega) - G_e}{\omega^2} = \int_0^\infty \tau H(\tau) d\tau < \infty, \tag{2.10}$$

$$\eta_0 = \lim_{\omega\to 0} \frac{G''(\omega)}{\omega} = \int_0^\infty H(\tau) d\tau < \infty, \tag{2.11}$$

$$G'_\infty = \lim_{\omega\to\infty} G'(\omega) = \int_0^\infty H(\tau)\frac{d\tau}{\tau} = G(0) < \infty. \tag{2.12}$$

In the case of a viscoelastic liquid, η_0 in (2.11) denotes the *zero shear-rate viscosity.*

Without loss of generality the constant G_e will be be set to zero. This is the relevant case for viscoelastic liquids. The addition of a constant term, $G_e > 0$, which is required in the case of viscoelastic solids, can be easily accommodated. The way in which the constraints (2.10)-(2.12) are built into the trial space for H will be made clear in Section 8.

3. Spectrum recovery as a deconvolution problem.

Equations (2.8) and (2.9) may be written in convolution form by choosing the logarithmic variable $x = \ln\omega$. Let

$$H(\omega^{-1}) = h(x), \quad G'(\omega) = \tfrac{1}{2}g_1(x), \quad \text{and} \quad G''(\omega) = \tfrac{1}{2}g_2(x). \tag{3.1}$$

Then, with $G_e = 0$, (2.8) and (2.9) become

$$g_1(x) = [1 + \tanh(x)] \star h(x), \tag{3.2}$$
$$g_2(x) = \operatorname{sech}(x) \star h(x), \tag{3.3}$$

where $\star$ denotes convolution, i.e.

$$(f \star g)(x) = \int_{-\infty}^{\infty} f(x-s)g(s)ds. \tag{3.4}$$

It is assumed throughout this article that $h(x) \in L^1(\mathbf{R}) \cap C(\mathbf{R})$ so that the Fourier transform $\hat{h}$ exists. The convention for the Fourier transform is

$$\widehat{h}(\xi) = \int_{-\infty}^{\infty} h(t)e^{-i\xi t}dt. \tag{3.5}$$

From (3.2) and (3.3) it may be shown that $g_1(x) \notin L^1(\mathbf{R})$ and $g_2(x) \in L^1(\mathbf{R}) \cap C(\mathbf{R})$. The Fourier transform of $g_1(x)$ exists only in the sense of distributions. Even so, equations (3.2) and (3.3) may be solved using the convolution theorem for Fourier transforms.

Differentiating (3.2) gives

$$Dg_1 = \operatorname{sech}^2(x) * h(x), \tag{3.6}$$

which, after Fourier transformation, reads

$$i\xi\widehat{g_1}(\xi) = 2\bar{\xi}\operatorname{cosech}\left(\bar{\xi}\right)\widehat{h}(\xi), \quad \text{where} \quad \bar{\xi} = \frac{\pi}{2}\xi.$$

It follows that

$$\widehat{h}(\xi) = \frac{1}{2}\bar{\xi}^{-1}\sinh\left(\bar{\xi}\right)i\xi\widehat{g_1}(\xi), \tag{3.7}$$

with continuity at $\xi = 0$. Similarly, noting that the transform of $\operatorname{sech}(x)$ is $\pi\operatorname{sech}\left(\bar{\xi}\right)$, it follows from (3.3) that

$$\widehat{h}(\xi) = \frac{1}{\pi}\cosh\left(\bar{\xi}\right)\widehat{g_2}(\xi). \tag{3.8}$$

Replacing the hyperbolic functions in (3.7) and (3.8) by their Maclaurin series, and inverting term by term, leads to solutions of (3.2) and (3.3) in the form

$$h(x) = h_1(x) + \frac{1}{\pi}\sum_{r=1}^{\infty}\frac{(-1)^r}{(2r+1)!}\bar{D}^{2r+1}g_1(x), \tag{3.9}$$

$$\text{and} \quad h(x) = h_0(x) + \frac{1}{\pi}\sum_{r=1}^{\infty}\frac{(-1)^r}{(2r)!}\bar{D}^{2r}g_2(x), \tag{3.10}$$

respectively, with

$$h_0(x) = \tfrac{1}{\pi} g_2(x), \quad h_1(x) = \tfrac{1}{2} D g_1(x) = \tfrac{1}{\pi} \bar{D} g_1(x), \tag{3.11}$$

where D, $\bar{D}$ denote the differential operators

$$D = \frac{d}{dx}, \quad \bar{D} = \frac{\pi}{2} D. \tag{3.12}$$

Sufficient conditions for the convergence of the series (3.9) and (3.10) will be given in Section 5, together with a proof of convergence.

4. Deconvolution of the complex modulus as a complex function: mixed series.

Rather than separate deconvolution of the real and imaginary parts of the complex modulus, which involves the inversion of real-valued kernels, it is of interest to consider its deconvolution as a complex function, which involves a complex-valued kernel. Consider, first, the hyperbolic identity

$$1 = \tfrac{1}{2}[\sinh(3\bar{\xi})\mathrm{cosech}(\bar{\xi}) - \cosh(3\bar{\xi})\mathrm{sech}(\bar{\xi})]. \tag{4.1}$$

Multiplying both sides of (4.1) by $\hat{h}(\xi)$ gives

$$\hat{h}(\xi) = \frac{1}{2\pi}[\sinh(3\bar{\xi})\xi^{-1}\widehat{\mathrm{D}g_1}(\xi) - \cosh(3\bar{\xi})\hat{g}_2(\xi)], \tag{4.2}$$

whereupon, by expanding the sinh and cosh functions and taking the inverse transform term by term, the following mixed series is obtained:

$$h(x) = \tfrac{3}{2} h_1(x) - \tfrac{1}{2} h_0(x) + \frac{1}{2\pi} \sum_{r=1}^{\infty} (-1)^r [\frac{3^{2r+1}}{(2r+1)!} \bar{D}^{2r+1} g_1(x) - \frac{3^{2r}}{(2r)!} \bar{D}^{2r} g_2(x)]. \tag{4.3}$$

Other mixed series of this type are derivable by employing hyperbolic identities of higher order than (4.1). What is of special interest about the series (4.3), however, is that it emerges from direct deconvolution of the complex equation

$$g_1(x) + i g_2(x) = [1 + \tanh(x) + i\mathrm{sech}(x)] \star h(x), \tag{4.4}$$

which is the subject of this section.

To derive (4.2) from (4.4), differentiate both sides of (4.4) and take the Fourier transform, to give

$$\widehat{Dg_1}(\xi) - \xi \hat{g}_2(\xi) = 2\bar{\xi}[\mathrm{cosech}(\bar{\xi}) - \mathrm{sech}(\bar{\xi})]\hat{h}(\xi). \tag{4.5}$$

Now, since h is real-valued, both $\hat{h}$ and $\widehat{Dg_1}$ are conjugate hermitian functions, while $\xi\widehat{g_2}(\xi)$ is anti-hermitian. It is no surprise, therefore, that equating the hermitian parts of (4.5) leads to (3.7), while equating the anti-hermitian parts leads to (3.8). On the other hand, expressing $\hat{h}$ in (4.5) in terms of the hermitian part of

$$\frac{\widehat{Dg_1}(\xi) - \xi\widehat{g_2}(\xi)}{2\bar{\xi}[\mathrm{cosech}(\bar{\xi}) - \mathrm{sech}(\bar{\xi})]}$$

leads to

$$\hat{h}(\xi) = \frac{1}{4\pi}[\sinh(3\bar{\xi}) + \sinh(\bar{\xi})]\xi^{-1}\widehat{\mathrm{Dg_1}}(\xi) - \frac{1}{4\pi}[\cosh(3\bar{\xi}) - \cosh(\bar{\xi})]\widehat{\mathrm{g_2}}(\xi). \quad (4.6)$$

Equation (4.2) now follows from (4.6) by simplifying the right-hand side using (3.7) and (3.8), and rearranging.

Notice that the identity (4.1) is the difference of two functions each with the same exponential growth. When the sinh and cosh functions are replaced by their series representations, the rates of growth of the partial sums are no longer the same. This property imposes more stringent convergence criteria on (4.3) than are required for the series (3.9) and (3.10).

5. Convergence.

The derivative series introduced so far have been derived in a formal manner. Sufficient conditions for convergence are required, and are provided in this section. More than one approach is possible in the study of sufficient conditions. (Loy *et al* (2017) treat a mollified series). Here we restrict attention to integrability conditions and dominated convergence. The following three sequences of partial sums are considered:
For $n = 1, 2, 3, \ldots,$

$$h_{2n+1}(x) = h_1(x) + \frac{1}{\pi}\sum_{r=1}^{n}\frac{(-1)^r}{(2r+1)!}\bar{D}^{2r+1}g_1(x), \quad (5.1)$$

$$h_{2n}(x) = h_0(x) + \frac{1}{\pi}\sum_{r=1}^{n}\frac{(-1)^r}{(2r)!}\bar{D}^{2r}g_2(x), \quad (5.2)$$

$$h^*_{2n+1}(x) = \tfrac{3}{2}h_1(x) - \tfrac{1}{2}h_0(x) + \frac{1}{2\pi}\sum_{r=1}^{n}(-1)^r[\frac{3^{2r+1}}{(2r+1)!}\bar{D}^{2r+1}g_1(x) - \frac{3^{2r}}{(2r)!}\bar{D}^{2r}g_2(x)], \quad (5.3)$$

First, in Theorem 5.1 below, conditions are given such that $h_{2n+1}(x) \to h(x)$ and $h_{2n}(x) \to h(x)$ as $n \to \infty$, for all $x \in \mathbf{R}$. The following standard results are used:

Lemma 5.1 Let f_1, f_2 be real-valued functions with Fourier transforms $\widehat{f_1}$, $\widehat{f_2}$. Let f_1 and $\widehat{f_2} \in L^1(\mathbf{R})$. [See Titchmarch (1948), Theorem 35, p54]. Then

$$\int_{-\infty}^{\infty} f_1(x-y)f_2(y)dy = \frac{1}{2\pi}\int_{-\infty}^{\infty} \widehat{f_1}(\xi)\widehat{f_2}(\xi)e^{ix\xi}d\xi. \tag{5.4}$$

Lemma 5.2 For any given $r \geq 0$, $\bar{D}^{2r}\mathrm{sech}(x)$ is a polynomial in odd powers of $\mathrm{sech}(x)$ of degree $2r+1$, and $\bar{D}^{2r}\mathrm{sech}^2(x)$ is a polynomial in even powers of $\mathrm{sech}(x)$ of degree $2r+2$.
This lemma is easily established by induction. It follows that $\bar{D}^{2r}\mathrm{sech(x)}$ and $\bar{D}^{2r}\mathrm{sech}^2\mathrm{(x)} \in \mathrm{L}^1(\mathbf{R}) \cap \mathrm{C}(\mathbf{R})$.

Theorem 5.1. Let $h \in L^1(\mathbf{R}) \cap C(\mathbf{R})$ and $\hat{h} \in L^1(\mathbf{R})$. Then $h_{2n+1}(x) \to h(x)$ and $h_{2n}(x) \to h(x)$ for all $x \in \mathbf{R}$.

Proof. For $n \geq 0$, let

$$F_{2n+1}(x) = \frac{1}{2}\sum_{r=0}^{n} \frac{(-1)^r}{(2r+1)!}\bar{D}^{2r}\mathrm{sech}^2\mathrm{(x)}, \tag{5.5}$$

so that

$$\widehat{F_{2n+1}}(\xi) = \sum_{r=0}^{n} \frac{\bar{\xi}^{2r+1}}{(2r+1)!}\mathrm{cosech}(\bar{\xi}). \tag{5.6}$$

Since $\bar{D}^{2r}\mathrm{sech}^2\mathrm{(x)} \in \mathrm{L}^1(\mathbf{R}) \cap \mathrm{C}(\mathbf{R})$ for all $r \geq 0$, and $h_{2n+1} = F_{2n+1} \star h$, it follows that $h_{2n+1} \in L^1(\mathbf{R}) \cap C(\mathbf{R})$. Hence, from (5.4),

$$h_{2n+1}(x) = \int_{-\infty}^{\infty} h(y)F_{2n+1}(x-y)dy = \frac{1}{2\pi}\int_{-\infty}^{\infty} \hat{h}(\xi)\widehat{F_{2n+1}}(\xi)e^{ix\xi}d\xi. \tag{5.7}$$

Now, $\hat{h}(\xi)\widehat{F_{2n+1}}(\xi)e^{ix\xi} \to \hat{h}(\xi)e^{ix\xi}$ for all $\xi \in \mathbf{R}$ as $n \to \infty$, and $|\hat{h}(\xi)\widehat{F_{2n+1}}(\xi)e^{ix\xi}| \leq |\hat{h}(\xi)|$. Hence, by dominated convergence, $h_{2n+1}(x) \to h(x)$ almost everywhere. But h and h_{2n+1} are continuous. Therefore $h_{2n+1}(x) \to h(x)$ for all $x \in \mathbf{R}$.

To prove that $h_{2n}(x) \to h(x)$ for all $x \in \mathbf{R}$, the same argument as above holds with $F_{2n+1}(x)$ and $\widehat{F_{2n+1}}(\xi)$ replaced by

$$F_{2n}(x) = \frac{1}{\pi}\sum_{r=0}^{n} \frac{(-1)^r}{(2r)!}\bar{D}^{2r}\mathrm{sech}(x) \quad \text{and} \quad \widehat{F_{2n}}(\xi) = \sum_{r=0}^{n} \frac{\bar{\xi}^{2r}}{(2r)!}\mathrm{sech}(\bar{\xi}). \tag{5.8}$$

The conditions for convergence stated in Theorem 5.1 are not sufficient to guarantee convergence of the sequence $h^*_{2n+1}(x)$ given by (5.3). To apply dominated convergence, an additional constraint on the decay rate of $\hat{h}(\xi)$ as $\xi \to \pm\infty$

is required. Let

$$A_n(x) = \frac{1}{4}\sum_{r=0}^{n}(-1)^r\frac{3^{2r+1}}{(2r+1)!}\bar{D}^{2r}\mathrm{sech}^2(\mathrm{x}) \tag{5.9}$$

$$\text{and} \quad B_n(x) = \frac{1}{2\pi}\sum_{r=0}^{n}(-1)^r\frac{3^{2r}}{(2r)!}\bar{D}^{2r}\mathrm{sech}(\mathrm{x}), \tag{5.10}$$

so that

$$\widehat{A_n}(\xi) = \frac{1}{2}\sum_{r=0}^{n}\frac{(3\bar{\xi})^{2r+1}}{(2r+1)!}\mathrm{cosech}(\bar{\xi}) \quad \text{and} \quad \widehat{\mathrm{B_n}}(\xi) = \frac{1}{2}\sum_{\mathrm{r=0}}^{\mathrm{n}}\frac{(3\bar{\xi})^{2\mathrm{r}}}{(2\mathrm{r})!}\mathrm{sech}(\bar{\xi}). \tag{5.11}$$

Then $\widehat{A_n}(\xi) \to A(\xi)$ and $\widehat{B_n}(\xi) \to B(\xi)$ for every $\xi \in \mathbf{R}$ as $n \to \infty$, where

$$A(\xi) = \tfrac{1}{2}\sinh(3\bar{\xi})\mathrm{cosech}(\bar{\xi}) \quad \text{and} \quad \mathrm{B}(\xi) = \tfrac{1}{2}\cosh(3\bar{\xi})\mathrm{sech}(\bar{\xi}). \tag{5.12}$$

Unfortunately, the condition $\hat{h} \in L^1(\mathbf{R})$ does not, in itself, guarantee that the sequence of functions $[\widehat{A_n}(\xi) - \widehat{B_n}(\xi)]\hat{h}(\xi)$ has a limit function in $L^1(\mathbf{R})$. However, such a limit exists for certain rapidly decaying functions $\hat{h}(\xi) \in L^1(\mathbf{R})$.

Definition. For $\sigma > 0$, h is said to belong to class $\mathcal{M}_\sigma$ if the following conditions pertain:
(i) $h \in L^1(\mathbf{R}) \cap C(\mathbf{R})$ and $\hat{h} \in L^1(\mathbf{R})$;
(ii) there exists a bounded, non-negative function $m(\xi) \in L^1(\mathbf{R})$, such that, for all $\xi \in \mathbf{R}$

$$|\hat{h}(\xi)| \le \mathrm{cosech}(\sigma\bar{\xi})\sinh(\bar{\xi})m(\xi) \quad \text{and} \quad |\hat{h}(\xi)| \le \mathrm{sech}(\sigma\bar{\xi})\cosh(\bar{\xi})m(\xi). \tag{5.13}$$

Examples.
(E1) For any constant λ, $\mathrm{sech}(\lambda\bar{\xi}) \in \mathcal{M}_\sigma$ if $\lambda > \sigma - 1$, and $\mathrm{sech}(\lambda\bar{\xi}) \notin \mathcal{M}_\sigma$ if $0 \le \lambda \le \sigma - 1$.
(E2) Certain non-negative band-limited functions are in $\mathcal{M}_\sigma$ for all $\sigma > 0$.
(E3) If h is in $\mathcal{M}_\rho$, then it is also in $\mathcal{M}_\sigma$ where $0 < \rho < \sigma$.

Theorem 5.2. Let $h \in \mathcal{M}_3$. Then $h^*_{2n+1}(x) \to h(x)$ for all $x \in \mathbf{R}$.

Proof. Again, this is a simple application of Lebesgue's dominated convergence theorem. For every $x \in \mathbf{R}$, and for every $\xi \in \mathbf{R}$,

$$[\widehat{A_n}(\xi) - \widehat{B_n}(\xi)]\hat{h}(\xi)e^{ix\xi} \to [A(\xi) - B(\xi)]\hat{h}(\xi)e^{ix\xi} = \hat{h}(\xi)e^{ix\xi}, \tag{5.14}$$

where the last step relies on the identity (4.3). Also

$$|[\widehat{A_n}(\xi) - \widehat{B_n}(\xi)]\hat{h}(\xi)e^{ix\xi}| \le [\widehat{A_n}(\xi) + \widehat{B_n}(\xi)]|\hat{h}(\xi)| \le m(\xi), \tag{5.15}$$

since $h \in \mathcal{M}_3$. Hence, by dominated convergence, as $n \to \infty$,

$$h^*_{2n+1}(x) = \frac{1}{2\pi}\int_{-\infty}^{\infty}[\widehat{A_n}(\xi) - \widehat{B_n}(\xi)]\hat{h}(\xi)e^{ix\xi}dx \to \frac{1}{2\pi}\int_{-\infty}^{\infty}\hat{h}(\xi)e^{ix\xi}dx = h(x).$$

6. Linearly mixed series: acceleration of convergence.

The series (4.3) is not a linear combination of (3.9) and (3.10), and its convergence requirements are restrictive. In contrast, mixed series derived from linear combinations share the same sufficiency conditions for convergence as the individual series (3.9) and (3.10). They can also be constructed to accelerate the convergence of the individual series.

Consider the functions $F_n(x)$, $n \geq 0$, defined by (5.5) and (5.8). We define F_n to be *order n*. The sequence $\{F_n(x)\}_{n=0}^{\infty}$ is a *delta-sequence*, i.e. a limit sequence for the Dirac delta distribution $\delta(x)$, with the property $\lim_{n\to\infty} \int_{-\infty}^{\infty} F_n(x)h(x)dx = h(0)$ for all $h \in L^1(\mathbf{R}) \cap C(\mathbf{R})$. Each F_n is symmetric, with a positive central peak at $x = 0$, which increases without limit, and becomes narrower as n increases. [See Figure 1]. Also, as a consequence of Lemma 5.2, any linear combination of F_{2n} and F_{2n+1} has at most 2n zeros.

For $n = 0, 1, 2, \ldots$, define the mixed, odd order sequence

$$h_{2n+1}^{\lambda} = F_{2n+1}^{\lambda} * h, \tag{6.1}$$

$$\text{where} \quad F_{2n+1}^{\lambda} = (1-\lambda)F_{2n} + \lambda F_{2n+1}, \tag{6.2}$$

for any real value of the parameter λ. Anderssen *et al* (2016) give reasons for choosing a value $\lambda = \frac{3}{2}$, and, with this value of λ, demonstrate the superior accuracy of the approximation h_1^{λ} compared with that of h_0 and h_1.

There is, however, no unique strategy for accelerating convergence of a series. One simple, but effective, approach is to choose λ so that F_1^{λ} is the best minimax approximation to F_2, and to keep this λ-value constant for all n. A suitable value of λ is 1.9, for which value the approximation h_{2n+1}^{λ} matches the accuracy of h_{2n+2}, not only for $n = 0$, but for all n of practical interest. In Figure 1, with $\lambda = 1.9$, the first three terms of the mixed delta-sequence F_{2n+1}^{λ} are compared with the first three terms of the delta-sequence F_{2n+2}. This is a clear demonstration of how lower order terms in a mixed sequence can match the resolution of higher order terms in an individual sequence.

The conceptual advantage of mixed series is generalized in Section 8 to mixed homeomorphic subspaces, and a case study is given in Section 9.

7. Native spaces.

The complex modulus $G^*(\omega)$ is analytic in the right-hand half-plane $Re\,\omega > 0$. Under the transformation $x = \ln(Re\,\omega)$, it follows that the data functions $g_1(x)$ and $g_2(x)$ are real analytic on $\mathbf{R}$. Douglas and Whittle Gruffudd (2016) have shown that if $\hat{g_2}$ extended to the complex plane is entire, there exists no h in $L^2(\mathbf{R})$ which has compact support, other than $h \equiv 0$. In this

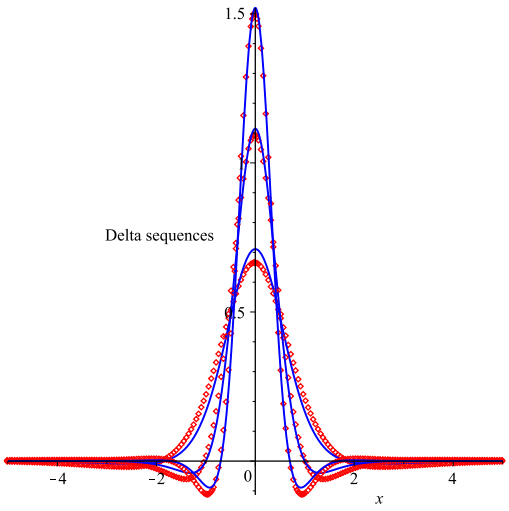

Figure 1: First three terms of the delta-sequence $F_1^\lambda, F_3^\lambda, F_5^\lambda, \ldots$ ($\diamond\diamond\diamond$), $\lambda = 1.9$, compared with the delta-sequence $F_2, F_4, F_6, \ldots$ (——).

paper, we treat functions $\hat{g_2}$ that do not have entire extension. Nevertheless, the advantage of working with h of non-compact support will become clear.

As mentioned earlier, an account of the native spaces in which g_1 and g_2 reside has not previously been given, and this will be done in this section. In the next section we identify certain subspaces of these native spaces which allow *deconvolution by homeomorphism*. For completeness, we begin with a brief summary of analytic models for g_1 and g_2 given by Davies and Goulding (2012) and Davies *et al* (2016).

Let $X = L^1(\mathbf{R}) \cap C(\mathbf{R})$ and $Y = L^1(\mathbf{R}) \cap C^\infty(\mathbf{R})$. Hence X and $Y \subset L^2(\mathbf{R})$. Furthermore let $S : X \to Y$, $T : X \to C^\infty(\mathbf{R})$ and $DT : X \to Y$ denote the convolution operators defined by

$$\begin{aligned} Sh(x) &= \operatorname{sech}(x) * h(x), && (7.1)\\ Th(x) &= [1 + \tanh(x)] * h(x), && (7.2)\\ \text{and} \quad DTh(x) &= \operatorname{sech}^2(x) * h(x), \quad h \in X. && (7.3) \end{aligned}$$

The inverse operators S^{-1}, T^{-1} and $(DT)^{-1}$, acting on the respective range spaces SX, TX and DTX, are not continuous. One approach to stabilizing the inversion is to choose a compact subset M of X such that S^{-1} is single-valued and continuous on the range space SM. In this case M and SM are homeomorphic subspaces. Similarly for the operators T and (DT). Usually, M is finite-dimensional. Moreover, if $\rho(.,.)$ denotes a metric in Y, and h is a function in M which minimizes the residual $\rho(Sh, g_2)$, then h is called *a quasi-solution*

of (3.3) (Ivanov (1962a,b)). In particular, one may write $h = S^{-1}Pg_2$, where P is the metric projection operator from Y to SM. Similarly for (3.2).

Davies and Goulding (2012) take M to be a finite-dimensional subspace of the trial space

$$X_\sigma = \text{span}\{\text{sech}(\frac{x-\alpha}{\sigma}) : \alpha \in \mathbf{R},\ \sigma \text{ fixed},\ 0 < \sigma < 1\}, \tag{7.4}$$

where the range of α is the whole of the reals and σ is a chosen scaling parameter. (The constraint $0 < \sigma < 1$ guarantees that the total viscosity of the model fluid is finite). A quasi-solution is found by discrete least-squares projection of the experimental data g_1 and g_2 onto TM and SM jointly. X_σ is a space of radial basis functions (RBFs), and as is often the case in RBF-approximation of experimental data, the numerical results are sensitive to both the dimension of M and the choice of scaling parameter σ.

In Davies *et al* (2016), the experimental data are first projected onto trial spaces constructed from weighted Gegenbauer polynomials which may be readily differentiated by means of a simple recurrence relation. To illustrate, consider a quasi-solution for h derived from the data g_2 by iterating the sequence (5.2) to convergence. Let λ be a half-integer chosen from the set $\{\frac{3}{2}, \frac{5}{2}, \frac{7}{2}, \dots\}$, let $C_n^{(\lambda)}(t)$ denote the Gegenbauer polynomial of degree n and order λ on $[-1, 1]$, and introduce an L^2-basis for Y given by $\{\gamma_{\sigma,n}^{(\lambda)}(x)\}_{n=0}^{\infty}$, where

$$\gamma_{\sigma,n}^{(\lambda)}(x) = \text{sech}^{\lambda-\frac{1}{2}}(\frac{x-\alpha}{\sigma})C_n^{(\lambda)}(\tanh(\frac{x-\alpha}{\sigma})). \tag{7.5}$$

Here, α denotes a fixed centering parameter and σ a fixed scaling parameter. The data g_2 are least-squares projected onto the $N+1$ dimensional subspace

$$Y_{\sigma,N}^{(\lambda)} = \text{span}\{\gamma_{\sigma,n}^{(\lambda)}(x) : n = 0, 1, 2, \dots, N\}, \tag{7.6}$$

and the quasi-solution h recovered in the space $S^{-1}Y_{\sigma,N}^{(\lambda)}$ by repeated use of the recurrence

$$D\gamma_{\sigma,n}^{(\lambda)}(x) = \sigma^{-1}[A_{n-1}\gamma_{\sigma,n-1}^{(\lambda)}(x) + B_{n+1}\gamma_{\sigma,n+1}^{(\lambda)}(x)], \tag{7.7}$$

where A_n and B_n are constants given by

$$A_n = \frac{n(n+2\lambda)}{2(n+\lambda+1)}, \quad B_n = -\frac{n(n+2\lambda)}{2(n+\lambda-1)}.$$

The parameters λ, N and σ affect the numerical stability of inversion and must be carefully chosen.

The trial spaces (7.4) and (7.6) can work well if the scaling parameters are correctly chosen, but this often requires repeated attempts by trial and

error. Moreover, they shed very little light on the true native spaces of the data g_1 and g_2. In this section, therefore, we provide characterizations of these native spaces, which then lead to an alternative approach to deconvolution by homeomorphism which is both more revealing and efficient than the methods based on (7.4) and (7.6).

Let $K : \mathbf{R} \times \mathbf{R} \to \mathbf{R}$, $K(x, y) = K(x - y)$, be a translation-invariant, symmetric positive definite kernel. Specific examples of such a kernel are those in (7.1) and (7.3), i.e., $\mathrm{sech}(x - y)$ and $\mathrm{sech}^2(x - y)$. Convolution integrals of type $K(x) * h(x)$ reside in the native space, $\mathcal{K}$, of the kernel K, which may be characterized in more than one equivalent form. The first of these is the completion of the trial space

$$\mathcal{K}_0 = \mathrm{span}\{K(x - \alpha) : \alpha \in \mathbf{R}\},$$

with respect to the inner-product

$$\langle \sum_{j=1}^{m} u_j K(\cdot - \alpha_j), \sum_{k=1}^{n} v_k K(\cdot - \beta_k) \rangle_{\mathcal{K}} = \sum_{j=1}^{m} \sum_{k=1}^{n} u_j v_k K(\alpha_j - \beta_k), \tag{7.8}$$

where $\{\alpha_1, \ldots, \alpha_m\}$ and $\{\beta_1, \ldots, \beta_n\}$ are any two sets of distinct points in $\mathbf{R}$. Further details may be found in Wendland (2005) and Schaback and Wendland (2006). We write

$$\mathcal{K} = \mathrm{clos}\ \mathcal{K}_0. \tag{7.9}$$

It follows from (7.8) that

$$\langle K(\cdot - \alpha), K(\cdot - \beta) \rangle_{\mathcal{K}} = \langle K(\cdot - \beta), K(\cdot - \alpha) \rangle_{\mathcal{K}} = K(\alpha - \beta), \tag{7.10}$$

and consequently, for all $f \in \mathcal{K}$, and $\alpha \in \mathbf{R}$,

$$\langle f, K(\cdot - \alpha) \rangle_{\mathcal{K}} = f(\alpha). \tag{7.11}$$

This *reproduction property* illustrates the important fact that $\mathcal{K}$ is a *reproducing kernel Hilbert space* (RKHS) with reproducing kernel K.

For convolution integrals, (7.8) extends to

$$\langle K * u, K * v \rangle_{\mathcal{K}} = \int_{-\infty}^{\infty} \int_{-\infty}^{\infty} u(x) v(y) K(x - y) dx dy, \tag{7.12}$$

where $(K * u)(x) = \int_{-\infty}^{\infty} K(x - y) u(y) dy$, with corresponding norm

$$\|K * u\|_{\mathcal{K}}^2 = \int_{-\infty}^{\infty} \int_{-\infty}^{\infty} u(x) u(y) K(x - y) dx dy. \tag{7.13}$$

For each integer $n \geq 1$, define the RKHS

$$M^n = \text{clos } M_0^n, \qquad M_0^n = \text{span}\{\mu_n^{-1}\text{sech}^n(x-\alpha) : \alpha \in \mathbf{R}\}, \tag{7.14}$$

where the normalization constants $\mu_n = \int_{-\infty}^{\infty} \text{sech}^n(x)dx$ are given by

$$\mu_1 = \pi; \quad \mu_{2n+1} = \frac{(2n)!\pi}{2^{2n}(n!)^2}, \quad \mu_{2n} = \frac{2^{2n}(n!)^2}{n(2n)!}, \quad n \geq 1. \tag{7.15}$$

For finite n, the normalization constants are, of course, redundant. However, their inclusion admits the sequence $\{\mu_n^{-1}\text{sech}^n(x)\}_{n=1}^{\infty}$ as a limit sequence for $\delta(x)$. In consequence, let M_0^{∞} denote the trial space of delta distributions

$$M_0^{\infty} = \text{span}\{\delta(x-\alpha) : \alpha \in \mathbf{R}\}. \tag{7.16}$$

From (3.3) and (3.6) it then follows that $g_2 \in M^1$, and $Dg_1 \in M^2$, with

Characterization 1. For $n = 1, 2$:

$$M^n = \{\text{sech}^n * h : h \in L^2(\mathbf{R}) \cup M_0^{\infty}, \int_{-\infty}^{\infty}\int_{-\infty}^{\infty} h(x)h(y)\text{sech}^n(x-y)dxdy < \infty\}.$$

The characterization admits both continuous and discrete spectra, and the spaces M^1 and M^2 are slightly larger than strictly required by the conditions on the data g_1 and g_2 imposed by Theorem 5.1. [Observe that if $h, \widehat{h} \in X$, then $h, \widehat{h} \in L^2(\mathbf{R})$]. In keeping with (7.8), $h(x)$ may take the form $\sum_k c_k\delta(x-\alpha_k)$, where $\sum_j \sum_k c_j c_k \text{sech}^n(\alpha_j - \alpha_k) < \infty$.

Note that, since $Dg_1 \in M^2$, then g_1 resides in the integrated space IM^2, where

$$IM^2 = \{f : Df \in M^2 \text{ and } f \to 0 \text{ as } x \to -\infty.\} \tag{7.17}$$

The second characterization follows from the first upon application of the Parseval-Plancherel formula to the double integral. Then $g_2 \in M^1$, and $Dg_1 \in M^2$, with

Characterization 2.

$$M^1 = \{f = \text{sech} * h : h \in L^2(\mathbf{R}) \cup M_0^{\infty}, \int_{-\infty}^{\infty} \cosh(\bar{\xi})|\widehat{f}(\xi)|^2 d\xi < \infty\}.$$

$$M^2 = \{f = \text{sech}^2 * h : h \in L^2(\mathbf{R}) \cup M_0^{\infty}, \int_{-\infty}^{\infty} \frac{\sinh(\bar{\xi})}{\bar{\xi}}|\widehat{f}(\xi)|^2 d\xi < \infty\}.$$

By expanding the above cosh term, for every finite N we have

$$\int_{-\infty}^{\infty} \sum_{r=0}^{N} \frac{\bar{\xi}^{2r}}{(2r)!} |\widehat{f}(\xi)|^2 d\xi = \sum_{r=0}^{N} \int_{-\infty}^{\infty} \frac{\bar{\xi}^{2r}}{(2r)!} |\widehat{f}(\xi)|^2 d\xi \tag{7.18}$$

$$= 2\pi \sum_{r=0}^{N} \int_{-\infty}^{\infty} \frac{|\bar{D}^r f|^2}{(2r)!} dx \tag{7.19}$$

$$< \int_{-\infty}^{\infty} \cosh(\bar{\xi}) |\widehat{f}(\xi)|^2 d\xi. \tag{7.20}$$

As $N \to \infty$, the first integral in (7.18) converges to the final integral in (7.20) by monotone convergence. Consequently, the two intermediate sums converge to the same integral. It follows that

$$\frac{1}{2\pi} \int_{-\infty}^{\infty} \cosh(\bar{\xi}) |\widehat{f}(\xi)|^2 d\xi = \sum_{r=0}^{\infty} \frac{1}{(2r)!} \|\bar{D}^r f\|^2_{L^2(\mathbf{R})}, \tag{7.21}$$

and by a similar argument,

$$\frac{1}{2\pi} \int_{-\infty}^{\infty} \frac{\sinh(\bar{\xi})}{\bar{\xi}} |\widehat{f}(\xi)|^2 d\xi = \sum_{r=0}^{\infty} \frac{1}{(2r+1)!} \|\bar{D}^r f\|^2_{L^2(\mathbf{R})}. \tag{7.22}$$

This leads to

Characterization 3.

$$M^1 = \{f = \text{sech} * h : h \in L^2(\mathbf{R}) \cup M_0^\infty, \sum_{r=0}^{\infty} \frac{1}{(2r)!} \|\bar{D}^r f\|^2_{L^2(\mathbf{R})} < \infty\}.$$

$$M^2 = \{f = \text{sech}^2 * h : h \in L^2(\mathbf{R}) \cup M_0^\infty, \sum_{r=0}^{\infty} \frac{1}{(2r+1)!} \|\bar{D}^r f\|^2_{L^2(\mathbf{R})} < \infty\}.$$

Note that in all cases, $h \in L^2(\mathbf{R}) \cup M_0^\infty$ implies that $\text{sech}^n * h \in L^2(\mathbf{R})$. All three characterizations give equivalent descriptions of the same RKHS.

Fasshauer and Ye (2011) establish the equivalence between the RKHS with translation-invariant, positive definite kernels, $K(x-y)$, and *generalized Sobolev spaces* of the type depicted by characterization 3. In their theory, series of type (7.21) and (7.22) define *generalized Sobolev norms*. The kernels K are embedded in the space, $\mathcal{S}'$, of Schwartz distributions, and are shown to be the Green's functions of certain associated differential operators. As special cases of their

general theory we may infer

$$\frac{1}{\pi}\sum_{r=0}^{\infty}(-1)^r\frac{1}{(2r)!}\bar{D}^{2r}\mathrm{sech}(x-y) \;=\; \delta(x-y), \qquad (7.23)$$

$$\text{and}\quad \frac{1}{2}\sum_{r=0}^{\infty}(-1)^r\frac{1}{(2r+1)!}\bar{D}^{2r}\mathrm{sech}^2(x-y) \;=\; \delta(x-y). \qquad (7.24)$$

8. Homeomorphic subspaces.

Equipped with the characterizations established in Section 7, arguably the most important consequence of Theorem 5.1 is the identification of a sequence of trial spaces for the spectrum, h, each successive member of the sequence containing functions of higher resolution. We first prove

Theorem 8.1 $\quad M^1 \subset M^2 \subset M^3 \subset \cdots \subset L^2(\mathbf{R})$.

Proof. To show that $M^1 \subset M^2$ it is enough to show that, for every $h \in L^2(\mathbf{R}) \cup M_0^\infty$, there exists a $u \in L^2(\mathbf{R})$ such that

$$f = \mathrm{sech} * h = \mathrm{sech}^2 * u, \quad \text{and} \quad \int_{-\infty}^{\infty}\frac{\sinh(\bar{\xi})}{\bar{\xi}}|\widehat{f}(\xi)|^2 d\xi < \infty. \qquad (8.1)$$

The function $\widehat{u}(\xi) = \xi^{-1}\tanh(\bar{\xi})\widehat{h}(\xi)$ is in $L^2(\mathbf{R})$, as is its inverse L^2-Fourier transform, $u(x)$. In addition, u satisfies the convolution equation in (8.1). Finally, since f is in M^1, it is in M^2 since $\int_{-\infty}^{\infty}\bar{\xi}^{-1}\sinh(\bar{\xi})|\widehat{f}(\xi)|^2 d\xi < \int_{-\infty}^{\infty}\cosh(\bar{\xi})|\widehat{f}(\xi)|^2 d\xi$.

Exactly similar arguments establish that $M^{2n} \subset M^{2n+1} \subset M^{2n+2}$. The Fourier transforms

$$\mathcal{F}[\mathrm{sech}^{2n+1}(x)] \;=\; \frac{2^{2n}}{(2n)!}\pi\prod_{r=1}^{n}[(\frac{2r-1}{2})^2+\frac{\xi^2}{2}]\mathrm{sech}(\bar{\xi}), \quad n \geq 1, \qquad (8.2)$$

$$\text{and}\quad \mathcal{F}[\mathrm{sech}^{2n}(x)] \;=\; \frac{2^{2n-1}}{(2n-1)!}\prod_{r=1}^{n-1}(r^2+\frac{\xi^2}{2})\bar{\xi}\mathrm{cosech}(\bar{\xi}), \quad n \geq 2, \qquad (8.3)$$

are useful.

The sequence of nested subspaces in Theorem 8.1 shares some of the properties of a multiresolution analysis (MRA) of the space $L^2(\mathbf{R})$ which plays a fundamental role in the theory of wavelets (Mallat (2009)). Thus

- each subspace is invariant under shifts of any size. In an MRA the shifts are dyadic.

- The subspace M^n has a basis which is close to a scaled version of the basis in M^1. In particular, for every $x \in \mathbf{R}$, there is a *dilation factor* $\lambda(n;x)$, with $\sqrt{n} \le \lambda(n;x) < n$, such that $\mathrm{sech}^n(x) = \mathrm{sech}(\lambda(n;x)x)$. In an MRA the dilation factor is independent of x, and is larger than n.
- The spatial resolution of functions in M^m is higher than of the those in M^n for $m > n$.
- The union of the nested subspaces is dense in $L^2(\mathbf{R})$.

Now let h and $\widehat{h}$ satisfy the conditions of Theorem 5.1. Since $g_2 \in M^1$ it follows from (5.2) that

$$h \in M^1 \cup \bar{D}^2 M^1 \cup \bar{D}^4 M^1 \cup \ldots.$$

But, by Lemma 5.2 we know that $\bar{D}^{2r}\mathrm{sech}(x)$ is a polynomial in odd powers of $\mathrm{sech}(x)$ of degree $2r+1$. Thus

$$h \in M^1 \cup M^3 \cup M^5 \cup \ldots.$$

By the same argument, since $Dg_1 \in M^2$ it follows from (5.1) and Lemma 5.2 that

$$h \in M^2 \cup M^4 \cup M^6 \cup \ldots.$$

Hence, as a set-theoretic extension of mixed series, we have

$$h \in M^1 \cup M^2 \cup M^3 \cup \ldots. \tag{8.4}$$

From the computational viewpoint, therefore, an appropriate trial space for h is a finite-dimensional subspace of the sum $M_0^1 + M_0^2 + M_0^3 + \ldots$.

Consider the constraints (2.10)-(2.12) on the low order moments of the relaxation spectrum $H(\tau)$. Write $H(\tau) = h(t)$, where $t = -\ln\tau$. The constraints on h, in order, are then

$$\int_{-\infty}^{\infty} h(t)e^{-2t}dt < \infty, \tag{8.5}$$

$$\eta_0 = \int_{-\infty}^{\infty} h(t)e^{-t}dt < \infty, \tag{8.6}$$

$$G'_\infty = \int_{-\infty}^{\infty} h(t)dt = \|h\|_{L^1(\mathbf{R})} < \infty. \tag{8.7}$$

For $n \ge 3$, the basis functions $\mathrm{sech}^n(t)$ in M_0^n satisfy all three constraints. However, constraint (8.5) is not satisfied when $n = 2$, and both (8.5) and (8.6)are not satisfied when $n = 1$. A simple change of basis in M_0^1 and M_0^2 resolves this issue. Consider the following triplets of basis functions:

$$u_1^{[\beta]}(t) = \frac{\mathrm{sech}(t) - \frac{1}{2}\mathrm{sech}(\beta)[\mathrm{sech}(t-\beta) + \mathrm{sech}(t+\beta)]}{1 - \mathrm{sech}^2(\beta)} \in M_0^1, \tag{8.8}$$

$$u_2^{[\beta]}(t) = \frac{\mathrm{sech}^2(t) - \frac{1}{2}\mathrm{sech}(2\beta)[\mathrm{sech}^2(t-\beta) + \mathrm{sech}^2(t+\beta)]}{1 - \mathrm{sech}(2\beta)\mathrm{sech}^2(\beta)} \in M_0^2. \tag{8.9}$$

where β is an adjustable positive parameter. $u_1^{[\beta]}(t)$ has a rate of decay $e^{-3|t|}$ as $t \to \pm\infty$, which is independent of β, while similarly, $u_2^{[\beta]}(t)$ has a rate of decay $e^{-4|t|}$. The functions $u_1^{[\beta]}$ and $u_2^{[\beta]}$, therefore, satisfy all three constraints, and serve as suitable bases in M_0^1 and M_0^2, respectively. More importantly, translations of (8.8) serves as a basis for a subspace of M_0^3, as does (8.9) for a subspace of M_0^4.

The basis functions $u_1^{[\beta]}$ and $u_2^{[\beta]}$ enjoy the following interesting properties:

- they are symmetric and bell-shaped;
- they are positive for all t, and for all $\beta > 0$;
- their width (resolution) is controlled by the parameter β;
- $u_1^{[\beta]}(t) \to \text{sech}^3(t)$ as $\beta \to 0$; $u_2^{[\beta]}(t) \to \text{sech}^4(t)$ as $\beta \to 0$;
- $u_1^{[\beta]}(t) \to \text{sech}(t)$ as $\beta \to \infty$; $u_2^{[\beta]}(t) \to \text{sech}^2(t)$ as $\beta \to \infty$.

We are now in a position to create homeomorphic subspaces which may be used for stable deconvolution of experimental data. Let M be a finite dimensional trial space for h, given by

$$M \subset M_0^1 + M_0^2 + M_0^3 + \ldots.$$

The corresponding trial spaces for g_1 and g_2 are, respectively,

$$\begin{aligned} TM &\subset TM_0^1 + TM_0^2 + TM_0^3 + \ldots, \\ \text{and} \quad SM &\subset SM_0^1 + SM_0^2 + SM_0^3 + \ldots. \end{aligned}$$

Since TM is also finite dimensional, the inverse map $T^{-1} : TM \to M$ is continuous, as is $S^{-1} : SM \to M$. The pairs of spaces (M, TM) and (S, SM) are therefore homeomorphic. Once the data g_1 and g_2 are projected onto the spaces TM and SM, respectively, the recovery of h in M is immediate.

Projection onto TM and SM is a straightforward exercise in nonlinear regression, since, for each $n \geq 1$, the image of M_0^n under the mapping T may be obtained explicitly, and similarly for the mapping S. We have

$$TM_0^1 = \text{span}\{1 + \tanh(\tfrac{1}{2}(x-\alpha)) : \alpha \in \mathbf{R}\}; \tag{8.10}$$

$$TM_0^2 = \text{span}\{1 + D[(x-\alpha)\coth(x-\alpha)] : \alpha \in \mathbf{R}\}; \tag{8.11}$$

$$TM_0^{2n+1} = \frac{\pi}{(2n)!\mu_{2n+1}} \prod_{r=1}^{n} [(2r-1)^2 - D^2] TM_0^1, \ n \geq 1; \tag{8.12}$$

$$TM_0^{2n} = \frac{2}{(2n-1)!\mu_{2n}} \prod_{r=1}^{n-1} (4r^2 - D^2) TM_0^2, \quad n \geq 2. \tag{8.13}$$

Under the mapping S, with continuity at $x = \alpha$ in all cases, we have

$$SM_0^1 = \text{span}\{\frac{2}{\pi}(x-\alpha)\text{cosech}(x-\alpha) : \alpha \in \mathbf{R}\}; \tag{8.14}$$

$$SM_0^2 = \text{span}\{\tfrac{1}{4}\pi\text{sech}^2(\tfrac{1}{2}(x-\alpha)) : \alpha \in \mathbf{R}\}; \tag{8.15}$$

$$SM_0^{2n+1} = \frac{\pi}{(2n)!\mu_{2n+1}} \prod_{r=1}^{n}[(2r-1)^2 - D^2]SM_0^1,\ n \geq 1; \tag{8.16}$$

$$SM_0^{2n} = \frac{2}{(2n-1)!\mu_{2n}} \prod_{r=1}^{n-1}(4r^2 - D^2)SM_0^2, \quad n \geq 2. \tag{8.17}$$

9. An example of spectrum recovery from experimental data.

As a case study we choose the data published by Honerkamp and Weese (1989) for a polybutadiene blend (PBD1). Estimates of the CRS recovered from this data have been determined by several methods, and a comparison of existing results appears in Davies *et al* (2016). All agree on a bimodal spectrum.

For convenience, the trial space M_0^n will be said to be *order n.* In general, any data set will contain values for G' and G'' for a finite number of sampled frequencies. The PBD1 data has 17 sampled frequencies. If the order of the trial space is too high, then a multi-modal distribution of relaxation times will result. The true number of modes should reflect the diversity of structure within the macromolecule, and the appearance of too many modes in the spectrum will be a mark of over-resolution. This is at its most obvious in the case of a discrete spectrum. A priori information about the macromolecule under investigation should always be taken into consideration, where possible. Also, some estimate of the noise level in the data will be of value. For PBD1 an estimate of the rms noise is about 2%.

Trial space M_0^∞. Although, in this paper, we are concerned with the CRS, nevertheless, a discrete spectrum can act as a guide in choosing the dimension of the trial space M, and can also render a lower bound estimate on the noise level in the data. As an initial step, therefore, we choose $M \in M_0^\infty$, with the spectrum and data represented as follows:

$$h^N = \sum_{k=1}^{N} a_k\delta(x-\alpha_k); \quad g_1^N = \sum_{k=1}^{N} a_k[1+\tanh(x-\alpha_k)]; \quad g_2^N = \sum_{k=1}^{N} a_k\text{sech}(x-\alpha_k).$$

Note that since ω^{-1} and τ have the dimension of time, we have the approximants $H(\tau) \approx h^N(-x)$, $G'(\omega) \approx \frac{1}{2}g_1^N(x)$ and $G''(\omega) \approx \frac{1}{2}g_2^N(x)$. For every trial space in this study, the functions g_1^N and g_2^N are fitted to the data using the

nonlinear regression algorithm of Levenberg-Marquardt.

The experimental data, G', G'', are shown in red on the right of Figure 2. Frequencies are sampled in the range $0.9 < \ln\omega < 7.0$, and the G''-data show a single maximum in the region of $\ln\omega = 4$. With dimension $N = 4$, the blue curves on the right denote the C^∞-approximants to the data, and the spiked functions on the left represent the recovered discrete spectrum $H(\tau)$. For purposes of illustration, the height of each spike is truncated to the value $10^{-1}a_k$. The dimension $N = 4$ allows an excellent fit to the data with a joint rms error-of-fit of 1.3%. Given that the spaces SM_0^∞ and TM_0^∞ have the highest resolving power of all the available trial spaces, the rms error of 1.3% can be taken as a lower bound for the noise level in the data. The predicted values of η_0 and G'_∞ are $\eta_0 = 1.41 \times 10^4$ and $G'_\infty = 1.36 \times 10^6$.

The forward maps S and T, together with the inverse maps S^{-1} and T^{-1}, are from $\mathbf{R}$ to $\mathbf{R}$. For this reason, the real analytic continuations of G' and G'' outside the measured frequency range are shown in Figure 2. One of the discrete spectral modes is located at $\ln\tau = -8.1$, outside the reciprocal frequency range $-7 < \ln\tau < -0.9$, with a corresponding relaxation time of $3 \times 10^{-4}s$. The contribution of this mode to the viscosity η_0 is less than 1%, but the contribution to G'_∞ is almost 30%.

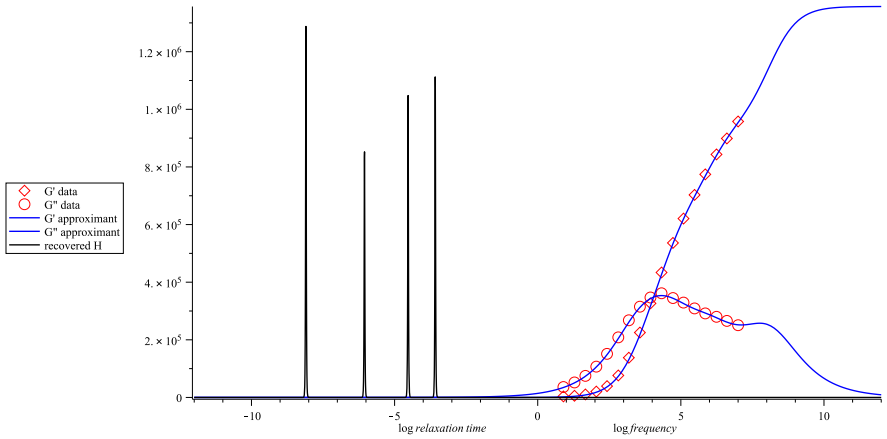

Figure 2: Recovery in a 4-dimensional subspace of M_0^∞. On the right: Experimental G' (◇ ◇ ◇); Experimental G'' (○ ○ ○); G', G''-approximants (—). On the left: Recovered 4-mode discrete spectrum(—).

Once the finite-dimensional trial space M is chosen, continuity of the inverse maps is guaranteed. However, numerical instabilities in regression can emerge if the dimension of M is too high. In the case of trial space M_0^∞, positivity of the coefficients a_k is required to preserve complete monotonicity

of the relaxation modulus $G(t)$. Positivity can be lost if $N > 4$.

Trial space M_0^3. Let M be chosen in M_0^3, with spectrum and data represented as follows:

$$\begin{aligned} h_3^N(x) &= \frac{2}{\pi}\sum_{k=1}^{N} a_k \mathrm{sech}^3(x-\alpha_k); \\ g_1^N(x) &= \sum_{k=1}^{N} a_k[1+\tfrac{3}{2}\tanh(\tfrac{1}{2}(x-\alpha_k)) - \tfrac{1}{2}\tanh^3(\tfrac{1}{2}(x-\alpha_k))]; \\ g_2^N(x) &= \frac{4}{\pi}\sum_{k=1}^{N} a_k[\coth(x-\alpha_k)\mathrm{cosech}(x-\alpha_k) - (x-\alpha_k)\mathrm{cosech}^3(x-\alpha_k)]. \end{aligned}$$

The above data-representations are found from (8.12) and (8.16), and it is understood that continuity is imposed at $x = \alpha_k$ in the case of g_2^N. In consequence, g_1^N and $g_2^N \in C^\infty(\mathbf{R})$. In this trial space it is not necessary that the coefficients a_k are all positive, only that $h_3^N(x)$ be positive for all x. The results for $N = 4$ are shown in Figure 3. The rms error-of-fit to the data is 2.1%. The recovered CRS is bimodal, in keeping with results from other methods. The predicted values of η_0 and G'_∞ are $\eta_0 = 1.1 \times 10^4$ and $G'_\infty = 1.2 \times 10^6$, both of which are lower than the values obtained from a discrete spectrum. Unlike the situation in Figure 2, the centres α_k all lie within the measured frequency range. One common feature of both trial spaces M_0^∞ and M_0^3 is that it is difficult to impose positivity on the spectrum when $N > 4$.

The triplet basis (8.8) spans a subspace of M_0^3 governed by the resolution parameter β. The basis for H in Figure 3 corresponds to the value $\beta = 0$. By increasing the value of β the rms error-of fit to the data reaches a minimum when $\beta \approx 0.35$, and thereafter increases once more. With a value $\beta = 0.35$, the spectrum H^β differs imperceptably from H at $\beta = 0$. However the rms error-of-fit is reduced from 2.1% to 1.8%. The result is shown on the left of Figure 4 in black, while the corresponding C^∞-approximants to the data are shown on the right in black. Also in Figure 4 are results from the trial space M_0^4.

Trial space M_0^4. In an attempt to improve resolution, consider $M \subset M_0^4$. In terms of the polynomials

$$p(t) = 1 + \tfrac{5}{2}t - \tfrac{3}{2}t^3; \quad q(t) = \tfrac{3}{2}(1-t^2)^2; \quad r(t) = \tfrac{3}{32}\pi t^2(2+t^2), \tag{9.1}$$

with continuity imposed at $x = \alpha_k$ where necessary, the spectrum and data are

represented as follows:

$$\begin{aligned} h_4^N(x) &= \tfrac{3}{4}\sum_{k=1}^{N} a_k \mathrm{sech}^4(x-\alpha_k); \\ g_1^N(x) &= \sum_{k=1}^{N} a_k[p(\coth(x-\alpha_k)) + (x-\alpha_k)q(\coth(x-\alpha_k))]; \\ g_2^N(x) &= \sum_{k=1}^{N} a_k r(\mathrm{sech}(\tfrac{1}{2}(x-\alpha_k))). \end{aligned}$$

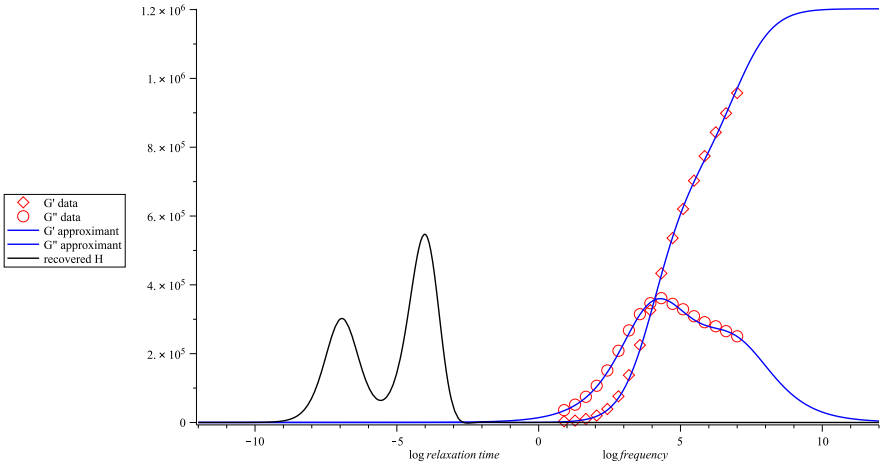

Figure 3: Recovery in a 4-dimensional subspace of M_0^3. On the right: Experimental G' (◇ ◇ ◇); Experimental G'' (○ ○ ○); G', G''-approximants (—). On the left: Recovered bimodal spectrum(—).

The spectrum $H_4^N(\tau) = h_4^N(-x)$ for $N = 4$ is shown on the left of Figure 4 in blue, with the corresponding C^∞-approximants to the data in blue on the right. There is an improvement in resolution of the spectrum, but the rms error-of-fit to the data is 2.6%, compared with 1.8% for $H^\beta(\tau)$. The values of η_0 are $\eta_0 = 1.19 \times 10^4$ for H_4^N compared with $\eta_0 = 1.1 \times 10^4$ for H^β, while the values of G'_∞ are $G'_\infty = 1.18 \times 10^6$ for H_4^N compared with $G'_\infty = 1.2 \times 10^6$ for H^β. Numerical investigations in the β-subspace of M_0^4 spanned by the basis (8.9) failed to reduce the rms-error of fit to the data to below 2.6%.

If an estimated rms noise level in the data of 2% is accepted, then, according to Morozov's discrepancy principle (Morozov, 1984), the best estimate of the spectrum derived from the data lies between the blue and black curves on the left of Figure 4, i.e. in the mixed trial space $M_0^3 + M_0^4$.

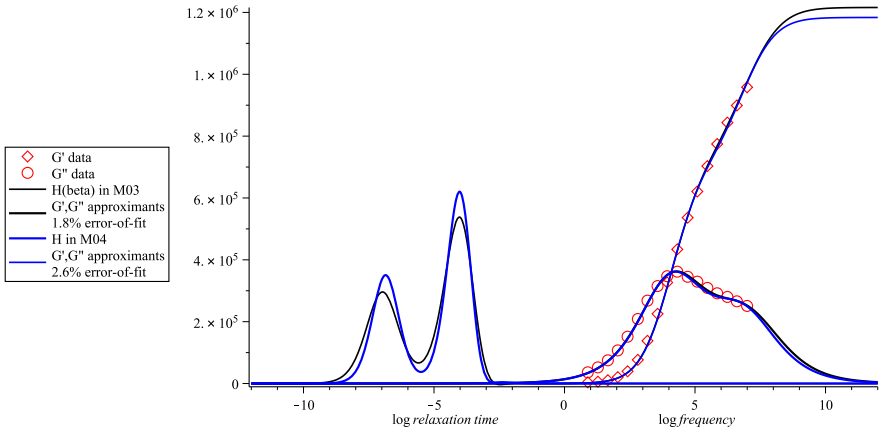

Figure 4: Recovery in 4-dimensional subspace of M_0^3 and M_0^4. On the right: Experimental G' ($\diamond\diamond\diamond$); Experimental G'' ($\circ\circ\circ$); G', $G''$with 2.6% error (—); G', $G''$with 1.8% error. (—) On the left: Recovered H^β in M_0^3 (—); recovered H in M_0^4(—).

The larger peak is centred at $\ln\tau \approx -4.1$, $\tau \approx 1.7 \times 10^{-2}$, in excellent agreement with other methods. The larger peak is centred in the range $-7.0 < \ln\tau < -6.6$, $9 \times 10^{-4} < \tau < 1.4 \times 10^{-3}$, again entirely consistent with other methods. Of interest is that the results presented here are free from small end-oscillations which are present in other methods.

A statement concerning overall accuracy of the recovered spectra is in order. The spectra shown in Figures 3 and 4 lie mainly within the interval $\ln\tau \in (-9, -2.5)$, which is partly outside the reciprocal range $\ln\tau \in (-7.0, -0.9)$ of the data. While the existence and position of the larger peak can be accepted with confidence, there is an element of uncertainty concerning the accuracy of the recovered spectra in the range $\ln\tau \in (-9, -7)$. This uncertainty is quantified by the accuracy of the analytic continuation of G' or G'' in the reciprocal interval $\ln\omega \in (7, 9)$, which is by no means easy to assess without further measurements being available.

10. Conclusion.

This paper presents, for the first time, an analysis of the native spaces of the storage and loss moduli (the real and imaginary parts of the complex modulus) in linear viscoelasticity. Sufficient conditions for convergence of inverse convolution operators in the form of differential series have been given, and the native spaces characterized in terms of these series as generalized Sobolev spaces. The inverse operators are then used to identify trial spaces for the continuous relaxation spectrum. Detailed homeomorphic trial spaces for data and spectrum are

constructed and are shown to deliver results for the spectrum which are in excellent agreement with other kernel methods, but which are easier to compute, without the need for selecting sensitive scaling parameters.

Acknowledgments

ARD acknowledges the support of EPSRC (UK) through the Inverse Problems Network grant EP/P005985/1. Sections 1 to 5 of this paper contain material translated from the Welsh language e-journal *Gwerddon*. We are pleased to acknowledge the source of this material (see Davies 2017). We thank three anonymous referees for their careful reading of the manuscript, and also thank Professors Karl-Michael Schmidt and Marco Marletta, Cardiff University, for useful and stimulating discussions.

References.

1. Anderssen, R.S., Davies, A.R., de Hoog, F.R. and Loy, R.J. (2015), Derivative based algorithms for continuous relaxation spectrum recovery. *Journal of Non-Newtonian Fluid Mechanics*, 222: 132-140.
2. Anderssen, R.S., Davies, A.R., de Hoog, F.R. and Loy, R.J. (2016), Simple joint inversion localized formulae for relaxation spectrum recovery. *The ANZIAM Journal*, 58:1-9.
3. Ankiewitz, S.,Orbey, N., Watanabe, H., Lentzakis, H. and Dealy, J. (2016), On the use of continuous relaxation spectra to characterize model polymers. *Journal of Rheology*, 60: 1115-1120.
4. Bernstein, S.N. (1928) Sur les fonctions absolument monotones. *Acta Mathematica* 52: 1-66.
5. Cho KS (2013), Power series approximations of dynamic moduli and relaxation spectrum. *J Rheol* 57: 679-697.
6. Davies, A.R. and Goulding, N.J. (2012), Wavelet regularization and the continuous relaxation spectrum. *Journal of Non-Newtonian Fluid Mechanics*, 189: 19-30.
7. Davies, A.R., Anderssen, R.S., de Hoog, F.R. and Goulding, N.J. (2016), Derivative spectroscopy and the continuous relaxation spectrum. *Journal of Non-Newtonian Fluid Mechanics*, 233: 107-118.
8. Davies, A.R. (2017) Deconvolution of the complex modulus in linear viscoelasticity. *Gwerddon* 24: 22-37. *In Welsh.*
9. Douglas R.J. and Whittle Gruffudd H.R. (2016), Nonexistence results for relaxation spectra with compact support. *Inverse Problems* 32: 035006 (13pp).
10. Fasshauer, G.E. and Ye, Q. (2011), Reproducing kernels of generalized Sobolev spaces using a Green function approach with distributional operators.*Numerische Mathematik* 119: 585-611.
11. Ferry, J.D. (1970). *Viscoelastic properties of polymers* (New York: Wiley).

12. Honerkamp, J, and Weese, J. (1989), Determination of the relaxation spectrum by a regularization method. *Macromolecules* 22:4372-4377.
13. Ivanov, V.K., (1962a) On linear problems which are not well-posed. *Soviet Math. Dokl.* 4: 981983
14. Ivanov, V.K., (1962b) On ill-posed problems. *Mat. Sb.* 61: 211223.(In Russian)
15. Loy, R.J.,de Hoog, F.R. and Anderssen R.S. (2017), Convergence in relaxation spectrum recovery. *Bulletin of the Australian Mathematical Society* 95: 121-132.
16. Malkin A Ya (2006), The use of a continuous relaxation spectrum for describing the viscoelastic properties of polymers.*Polymer Science Series A* 48:39-45.
17. Mallat, S. (2009), *A Wavelet Tour of Signal Processing. The Sparse Way* (San Diego: Academic Press).
18. McDougall, I., Orbey, N., and Dealy, J. (2014), Inferring meaningful relaxation spectra from experimental data. *Journal of Rheology,* 58: 770-797.
19. Morozov, V.A. (1984) *Methods for solving incorrectly posed problems.*(translated by Nashed, M.Z.). (New York, Springer).
20. Saut, J.C, and Joseph, D.D.(1983), Fading memory. *Archive for Rational Mechanics and Analysis*, 81: 53-95.
21. Schaback, R. and Wendland, H. (2006), Kernel techniques: from machine learning to meshless methods. *Acta Numerica*: 1-97.
22. Stadler FJ, Bailly C (2009). A new method for the calculation of continuous relaxation spectra from dynamic-mechanical data. *Rheologica Acta* 48:33-49.
23. Stadler F (2010). Effect of incomplete datasets on the calculation of continuous relaxation spectra from dynamic-mechanical data. *Rheologica Acta* 49:1041-1057.
24. Tanner, R.I. and Walters, K. (1998), *Rheology: An Historical Perspective* (Amsterdam: Elsevier).
25. Titchmarsh, E.C. (1948) *Introduction to the Theory of Fourier Integrals, 2nd edition* (Oxford University Press, UK).
26. Tschoegl, N.W. (1989),*The Phenomenological Theory of Linear Viscoelastic Behaviour* (Berlin Heidelberg: Springer-Verlag).
27. Walters, K. (1975) *Rheometry* (London: Chapman and Hall).
28. Wendland, H. (2005) *Scattered data approximation.* (Cambridge University Press, UK).